Zhang et al. *Zool. Res.* 2025, 46(4): 825−840
https://doi.org/10.24272/j.issn.2095-8137.2025.034
https://cstr.cn/32248.14.zr.2025.034

ZR | Zoological Research

Article Open Access

Phenotypic, transcriptomic, and genomic analyses reveal the spatiotemporal patterns and associated genes of coarse hair density in goats

Ji-Pan Zhang[1,2,3], Min Xiao[1,2,3], Jia-Bei Fang[1], De-Li Huang[4], Yong-Ju Zhao[1,2,3,*]

[1] *College of Animal Science and Technology*, *Southwest University*, *Chongqing* 400715, *China*
[2] *Chongqing Key Laboratory of Herbivore Science*, *Chongqing* 400715, *China*
[3] *Chongqing Key Laboratory of Forage & Herbivore*, *Chongqing* 400715, *China*
[4] *Tengda Animal Husbandry Co.*, *Ltd.*, *Chongqing* 402360, *China*

ABSTRACT

The genetic regulation of hair density in animals remains poorly understood. The Dazu black goat, characterized by its black coarse hair and white skin, provides a unique model for dissecting coarse hair density (CHD). Using high-resolution micro-camera imaging, this study analyzed 905 skin images, 33 skin transcriptomes, 272 whole-genome sequences, and 182 downloaded transcriptomes. Morphological assessment from juvenile to adult stages revealed the thickening of hair shafts accompanied by a progressive decline in density, largely attributable to rapid surface expansion of the trunk skin. Transcriptomic comparison between high- and low-CHD individuals identified 572 differentially expressed genes (DEGs). A genome-wide association study detected 25 significant single nucleotide polymorphisms (P<9.07e-8) and mapped 48 annotated genes, with the most prominent association signal located near *GJA1* on chr9.15931585-18621011. Literature review and Venn analysis highlighted six genes (*GJA1*, *GPRC5D*, *CD1D*, *CD207*, *TFAM*, and *CXCL12*) with documented roles in skin and hair biology, and three genes (*GJA1*, *GPRC5D*, and *ATP6V1B1*) overlapped with DEGs. Multiple-tissue transcriptomic profiling, western blotting, immunohistochemical staining, and skin single-cell RNA sequencing confirmed that *GJA1* and *GPRC5D* were highly and specifically expressed in skin, particularly within hair follicles. Expression was localized predominantly to follicular stem cells and dermal papilla cells, suggesting a significant role in folliculogenesis and structural maintenance. Cross-validation using four public datasets further demonstrated positive correlations between *GJA1* and *GPRC5D* expression and hair follicle density. The innovative micro-camera application allowed the elucidation of spatiotemporal patterns and genes associated with CHD, thereby addressing a significant knowledge gap in animal hair density.

Keywords: Goat; Hair density; Spatiotemporal pattern; Skin image; GWAS; *GJA1*

INTRODUCTION

Hair follicles are dynamic epithelial-mesenchymal structures in mammals characterized by cyclic phases of growth and continuous regeneration throughout life (Paus & Cotsarelis, 1999; Wu et al., 2024). Most hair follicles originate during embryonic development, regulated by complex signaling between the ectoderm and mesoderm (Schneider et al., 2009). Goats exhibit two hair follicles populations with distinct morphological and physiological features, namely primary hair follicles and secondary hair follicles (Zhang et al., 2020a). Primary hair follicles are larger in size, more sparsely distributed, and produce coarse guard hairs that provide physical protection, while secondary hair follicles are smaller, denser, and generate cashmere fibers essential for thermoregulation (Yang et al., 2019). Hair follicles undergo continuous cycling through three defined phases: anagen (active growth), catagen (regression), and telogen (quiescence) (Yang et al., 2020). In fiber- and fur-producing species such as goats, sheep, rabbits, alpacas, and mink, fiber yield and coat quality are largely determined by fiber density. Hair density is modulated by multiple factors, including breed (Zhang et al., 2019), sex (Ansari-Renani et al., 2012), seasonal variation (Mirmahmoudi et al., 2017), and pharmacological treatment (Diao et al., 2023). Despite its

Received: 20 May 2025; Accepted: 16 June 2025; Online: 17 June 2025
Foundation items: This work was supported by the National Key Research and Development Program of China (2022YFD1300202), Collection, Utilization, and Innovation of Animal Resources by Research Institutes and Enterprises of Chongqing (Cqnyncw-kqlhtxm), Chongqing Modern Agricultural Industry Technology System (CQMAITS202413), and National Training Program of Innovation and Entrepreneurship for Undergraduates (S202310635040)

*Corresponding author, E-mail: zyongju@163.com

economic importance, the genetic mechanisms underlying variation in hair density remain poorly characterized.

Advances in next-generation sequencing technologies have enabled comprehensive exploration of the genomic and transcriptomic landscapes associated with complex traits. Genome-wide association study (GWAS) is a powerful tool for identifying genomic loci and variants linked to phenotypic variation (Hirschhorn & Daly, 2005; Mccarthy et al., 2008), and have been successfully applied in goats to investigate economically important traits, such as body morphology (Gu et al., 2022; Rong et al., 2025; Yang et al., 2024), cashmere length, and hair diameter (Lu et al., 2024; Rong et al., 2024; Zhang et al., 2025b). Similarly, transcriptomic profiling through mRNA sequencing (mRNA-seq) has facilitated the identification of differentially expressed genes (DEGs) in response to various stimuli, such as changes in photoperiod length (Yang et al., 2017), melatonin exposure (Diao et al., 2025; Li et al., 2022), and breed-specific factors (Zhang et al., 2019). These advances offer a promising foundation for deciphering the key genetic determinants of hair density in goats through integrated genomic and transcriptomic analyses.

Quantitative assessment of hair density is essential for elucidating its genetic basis. Conventional histological methods employing hematoxylin-eosin (H&E) (Liu et al., 2021) or Sacpic staining (Diao et al., 2023; Nixon, 1993) provide high-resolution visualization of follicle structure but are invasive, labor-intensive, and unsuitable for large-scale phenotyping in live animals. In contrast, micro-camera technology offers a non-invasive and scalable alternative for capturing high-resolution skin images, facilitating efficient hair density quantification. The Dazu black goat, a meat-type breed originating from southwestern China, exhibits black coarse hair on white skin (Guan et al., 2016; Zhang et al., 2025b) and a moderate body size (Figure 1A), making it an ideal model for large-scale investigation and genetic identification of coarse hair density (CHD).

This study investigated the spatiotemporal dynamics of CHD and identified associated functional genes through an integrated genomic and transcriptomic framework. CHD was first quantified across 10 anatomical regions in 60 goats spanning multiple developmental stages to characterize spatial and age-related variation. Subsequently, skin transcriptomes from 33 adult goats and whole-genome sequences from 272 adult goats were analyzed to identify candidate genes linked to CHD. Final validation incorporated a literature review, multi-tissue expression analysis, western blotting, immunohistochemistry, skin single-cell transcriptomics, and extended transcriptomic datasets from individuals with divergent hair follicle densities.

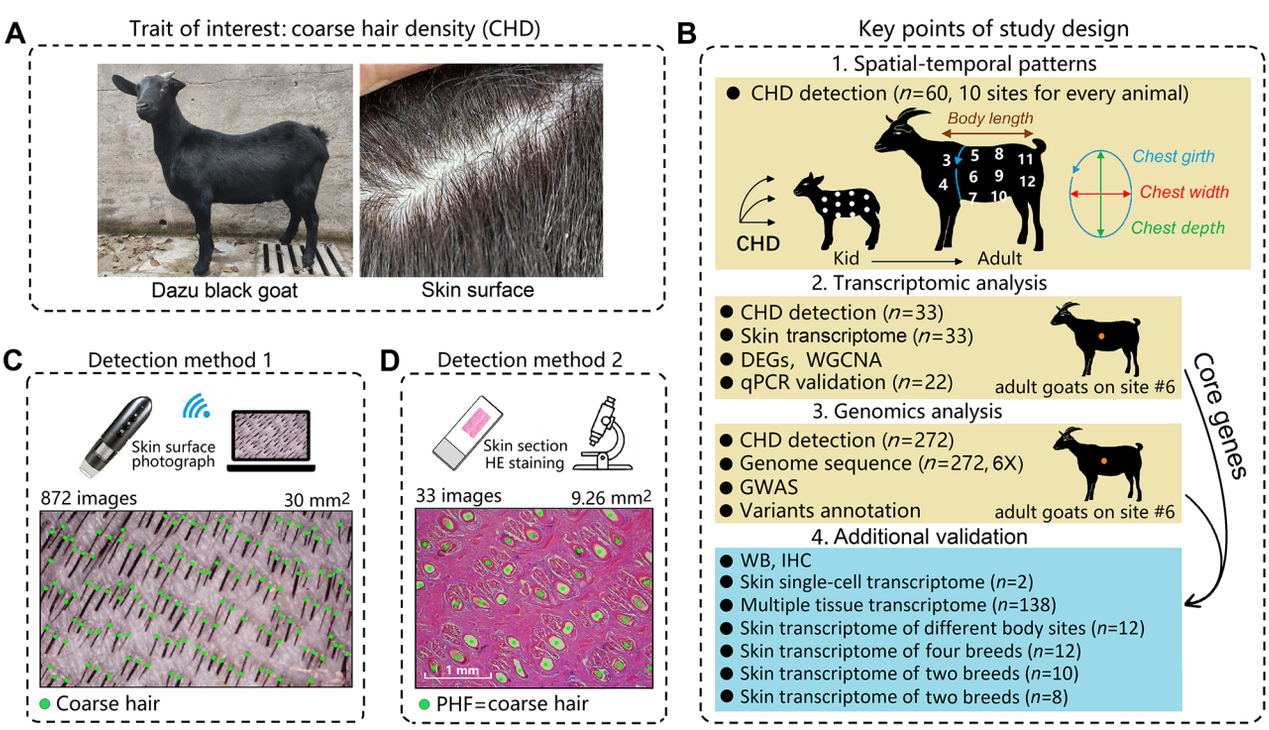

Figure 1 Study design and methods for CHD detection

A: Representative images of Dazu black goat and its skin surface. The strong contrast between coarse black hair and white skin provides an optimal model for studying coarse hair density (CHD). B: Overview of study design. The complete workflow is provided in Supplementary Figure S1. CHD was measured at 10 anatomical sites in 60 goats spanning developmental stages from kid to adult. These body sites included (#3) upper shoulder, (#4) forearm, (#5) dorsal chest, (#6) lateral chest, (#7) posterior chest, (#8) dorsal waist, (#9) lateral abdomen, (#10) ventral abdomen, (#11) croup, and (#12) thigh. Skin transcriptome sequencing was performed on 33 samples to identify DEGs associated with CHD. Whole-genome sequencing was conducted on 272 adult goats to identify genomic variants and annotated genes associated with CHD. Additionally, 182 publicly available transcriptomes were analyzed to explore candidate gene expression profiles. C: Non-invasive CHD detection method. Coarse hair was clipped using an electric clipper, and a 30 mm^2 skin image was captured using a micro-camera. Each green dot represents a single coarse hair. D: Histological CHD assessment. Paraffin-embedded skin sections were stained with H&E, and a 9.26 mm^2 area was imaged. Each green dot represents a primary hair follicle, which produces one coarse hair.

MATERIALS AND METHODS

Animals and study design

All experimental procedures were approved by the Animal Care and Use Committee of Southwest University (No. IACUC-20230417-02). A total of 365 goats were included in the study and maintained on a standard artificial diet composed of alfalfa, barley grain, and wheat straw. Feed composition was balanced according to the nutritional guidelines established for goats by the National Research Council (2007). An overview of the experimental workflow and study design is provided in Supplementary Figure S1 and Figure 1B, respectively. The study was conducted in four sequential phases: characterization of spatiotemporal patterns of CHD, transcriptomic profiling, genome-wide analysis, and multi-level validation.

(1) Group 1 consisted of 60 goats (13 males and 47 females, Figure 1B1) reared at the Southwest University farm (Chongqing, China), representing five developmental stages: lactating kid (1–3 months, *n*=14), early-fattening (3–6 months, *n*=15), mid-fattening (6–12 months, *n*=5), late-fattening (12–18 months, *n*=17), and adult (>18 months, *n*=9). For each animal, CHD was determined at body sites #3–12 (Supplementary Figure S2), as previously defined (Zhang et al., 2020a). A well-trained experimenter conducted site selection and captured standardized high-resolution skin images to ensure sampling precision. Body weight and morphological traits were also recorded. This dataset was used to investigate the spatial distribution of CHD and its temporal variation from kids to adults.

(2) Group 2 included 33 adult female goats (1.5–2.5 years old, Figure 1B2) reared and commercially slaughtered at Tengda or Ruifeng farms (Chongqing, China). Skin tissue from site #6 was collected for histological analysis and mRNA-seq. Body conformation traits were also recorded. This group was used to identify CHD-related genes through transcriptomic analysis.

(3) Group 3 comprised 272 adult female goats (>1.5 years old, Figure 1B3) reared at Southwest University or Tengda farms. CHD was measured at site #6, and blood samples were collected via jugular venipuncture for whole-genome sequencing. Body conformation traits were also recorded. This group was used to identify CHD-related genes through GWAS.

(4) In the validation phase, western blotting and immunohistochemistry were conducted to determine protein expression of candidate genes. Additionally, 182 publicly available transcriptomes (Figure 1B4) were analyzed to determine gene expression profiles across different skin cell types, multiple tissues, anatomical locations, and goat breeds. These datasets were used to observe the expression characteristics of the candidate genes we screened. Finally, we executed a comprehensive evaluation of the candidate genes by integrating multiple lines of evidence. These included whole-genome variation signals, differential transcriptional expression, tissue-specificity, protein expression, supporting literature evidence, and involvement in the biological functions of key hair follicle cells.

Determination of CHD

A novel, non-invasive approach was developed to quantify CHD (Figure 1C). Animals were manually restrained in a standing position, and a 5 cm×5 cm area of skin centered on each target site was shaved using an electric clipper (FC5902, Flyco, China), leaving stubble approximately 0.5–1 mm in length. Each stubble corresponded to a single hair shaft. High-resolution images of the shaved skin surface were captured using a micro-camera (Xifeng, China) equipped with a built-in light source and pre-fixed focal length. The physical area of the captured image was consistently 30 mm^2 (Supplementary Figure S3). The clearest and most representative image per site was retained for analysis. A total of 872 high-definition images were obtained (10 body sites from 60 goats in Group 1 and site #6 from 272 goats in Group 3). Using Image-Pro Plus v.6.0 (Media Cybernetics, USA), each visible hair stubble was marked with a green dot (Figure 1C). For consistency, two partially visible shafts at image margins were counted as one. The annotated images were processed using a custom in-house MATLAB script (R2018a MathWorks, Natick, USA) to extract and quantify the color-labeled stubbles.

For Group 2 animals, a conventional histological method was employed (Figure 1D). Skin tissue from site #6 was collected, fixed, dehydrated, embedded, sectioned, stained with H&E, and imaged, as described in our previous publication (Zhang et al., 2020a). Primary hair follicles were identified and labeled with green dots in Image-Pro Plus v6.0. Skin shrinkage was set at 0.7, representing the ratio of the stained histological area to the corresponding physiological skin surface area. This factor was used to adjust CHD values for samples in Group 2.

Determination of body weight and body conformation traits

Body weight (BW, kg) and four body conformation traits, including body length (BL, cm), chest girth (CG, cm), chest depth (CD, cm), and chest width (CW, cm), were recorded for all animals. BW was measured using an electronic platform scale with an accuracy of ±0.1 kg. BL was defined as the horizontal distance from the shoulder area to the pin bone. CG was measured as the circumference behind the shoulder blades in a vertical plane, perpendicular to the longitudinal body axis. CD represented the vertical plane depth of the chest, perpendicular to the longitudinal body axis. CW denoted the horizontal width of the chest, perpendicular to the longitudinal body axis (Ofori et al., 2021). Trunk surface area (TSA, cm^2) was calculated to represent the relative size of the animal surface area of the trunk, as shown below:

$$\mathrm{ThCG} = 2b + 4 \times (a - b) \tag{1}$$

$$\mathrm{TSA} = \frac{\mathrm{ThCG} + \mathrm{CG}}{2} \times \mathrm{BL} \tag{2}$$

$$\text{Total coarse hair on trunk} = \mathrm{TSA} \times \frac{\sum_{i=3}^{12} \mathrm{CHD}_i}{10} \tag{3}$$

where *a* and *b* represent the maximum and minimum values of CW and CD, respectively. Theoretical chest girth (ThCG) was calculated using Equation 1. TSA was then estimated using BL and arithmetic mean of ThCG and CG, as shown in Equation 2. Total coarse hair count on the trunk were determined by multiplying TSA and the mean CHD across 10 sampling sites, as defined in Equation 3, where *i* represents the site number.

Spatiotemporal patterns of CHD

The spatial distribution of CHD across the body and its temporal dynamics from the kid to adult stages were

systematically analyzed. To adjust for differences in body size, TSA was first calculated for each goat. CHD was then measured at 10 predefined body sites across five developmental stages: lactating kid, early-fattening, mid-fattening, late-fattening, and adult. For each anatomical site, age-dependent changes in CHD were examined. One-way analysis of variance (ANOVA) was performed to assess CHD differences among body sites. To evaluate potential sex effects, CHD values from 13 males and 13 females with closely matched TSA values were compared. Finally, the relationships among body conformation traits, BW, and mean_CHD (mean of 10 CHD values from #3–12 sites) were analyzed across developmental stages. Pearson correlations between CHD at site #6 and mean_CHD were calculated to confirm the suitability of site #6 as a representative sampling location for downstream analyses.

mRNA-seq and DEG analysis

Skin tissue was collected from 33 adult goats slaughtered at a local abattoir by jugular exsanguination. Prior to slaughter, hair at site #6 was trimmed using an electric clipper (Flyco, China). Immediately postmortem, two samples were harvested per animal. One sample was preserved in RNAstore reagent (CWbio, China) at −80°C for RNA extraction, and the other was immersed in a 4% paraformaldehyde fixing solution (Servicebio, China) for paraffin embedding and histological analysis. The 33 samples were assigned into high-, med-, and low-CHD groups according to their CHD values.

Total RNA was extracted from the 33 skin samples, and libraries were constructed by Lianchuan Biotechnology (China). Paired-end sequencing (150 bp) was performed using the Illumina platform (USA). Raw sequencing reads were processed with Trimmomatic (Bolger et al., 2014) to remove adapter and low-quality sequences reads. Clean reads were aligned to the *Capra* ARS1.2 reference genome (Bickhart et al., 2017) using STAR (Dobin et al., 2013). Transcript abundance was quantified with StringTie (Pertea et al., 2016) and normalized as fragments per kilobase of transcript per million mapped reads (FPKM). DEGs were identified using thresholds of $P<0.05$ and fold change (FC)≥1.5. Samples were ranked according to their CHD values, and those with the highest and lowest values were selected for differential expression analysis. To ensure robustness, comparisons were performed using varying numbers of biological replicates, ranging from six to 11 individuals per group. DEGs identified in each replicate set were then intersected to extract a subset of genes consistently differentially expressed across all comparisons, defined as the core DEGs.

qPCR validation and weighted gene co-expression network analysis (WGCNA)

To validate the expression levels of genes, 29 DEGs were subjected to quantitative polymerase chain reaction (qPCR). Total RNA extraction, reverse transcription, and qPCR analysis were performed according to previously described protocols, with *NCBP3*+*SDHA*+*PTPRA* used as the reference for normalization (Zhang et al., 2020b). Primer pairs of the 29 target genes and three reference genes were designed using Primer-BLAST (Ye et al., 2012) on the National Center for Biotechnology Information (NCBI) website. Detailed primer sequences and amplification efficiencies are provided in Supplementary Table S1. WGCNA was performed using the SangerBox platform (Shen et al., 2022) to identify key gene modules related to CHD. Correlation coefficients between gene modules and CHD traits were calculated, and key modules with $P<0.05$ were retained. The intersection of DEGs and core genes identified by WGCNA was determined. Functional enrichment of the overlapping genes was performed using Gene Ontology (GO) and Kyoto Encyclopedia of Genes and Genomes (KEGG) annotations with the OmicShare platform (https://www.omicshare.com/).

Genome sequencing, genotyping, and quality control

Blood samples from Group 3 goats were collected via jugular venipuncture and immediately stored at −80°C. DNA extraction, library preparation, and sequencing were performed by Compson Biotechnology Company (China) using the DNBSEQ-T7 platform (BGI, China). Genomic data for 124 goats were reported in our previous study (PRJNA786385 (Gu et al., 2022), while data for the remaining 148 goats are newly reported in this study. BWA v.0.7.15 (Li and Durbin, 2009), Picard v.1.129 (https://broadinstitute.github.io/picard), SAMtools v1.10 (Li et al., 2009), and GATK v.3.4.46 (Mckenna et al., 2010) were used for read mapping, duplicate elimination, sequence sorting, and single nucleotide polymorphism (SNP) calling, respectively. The variants were functionally annotated using snpEff v.5.1 (Cingolani et al., 2012). Quality control was performed using PLINK v.1.0.7 (Chang et al., 2015), with the filtering criteria set as described in previous studies (Luigi-Sierra et al., 2020; Zhao et al., 2022). SNPs that met the following requirements were removed: (i) SNPs without chromosomal or physical locations or located on sex chromosomes; (ii) SNPs with missing genotypes >0.1; (iii) SNPs with minor allele frequency <0.05; (iv) SNPs with a significant deviation ($P<0.001$) from the Hardy-Weinberg equilibrium. Individuals with a genotyping rate <90% were excluded.

Genome-wide association study (GWAS)

To account for population structure, principal component analysis (PCA) and relatedness analysis were performed prior to GWAS. PCA was conducted using PLINK v.0.76 (Chang et al., 2015) and the kinship matrix was calculated using GEMMA v.0.98.5 (Zhou & Stephens, 2012). A linear mixed model (LMM) was applied for SNP-trait association testing using GEMMA v.0.98.5, as represented in Equation 4 (Zhou & Stephens, 2012). To account for the potential influence of body conformation on CHD, a separate GWAS was performed using CHD_norm, defined as the CHD value normalized by the TSA value (Equation 5).

$$y = W\alpha + x\beta + Zu + e \tag{4}$$

$$\text{CHD\_norm} = \text{CHD} \times \frac{\text{TSA}}{\sum_1^{272}\text{TSA}_i/272} \tag{5}$$

where y denotes the vector of morphological traits; W represents the matrix of covariates, including fixed effects, such as age, farm, and the top 20 principal components (PCs); α is the vector of corresponding coefficients; x is the vector of SNP genotypes; β is the SNP effect size; Z is an incidence matrix accounting for relatedness; u is the vector of random effects; and e is the residual effect. The likelihood ratio test and Wald test were performed using GEMMA to evaluate the null hypothesis (β=0); i represents the serial number of 272 goats. A genome-wide significance threshold of P<9.07e-8 (1/11025802) was applied. Manhattan and quantile-quantile plots (QQ-plot) were generated using the qqman (Turner, 2018) and CMplot (Yin et al., 2021) packages,

respectively. Candidate genes located within ±500 kb of significant SNPs were identified using the biomaRt tool (Smedley et al., 2015).

Literature review and Venn analysis

To evaluate the functional relevance of candidate genes, literature mining was performed for each of the 48 candidate genes identified from SNP-GWAS, using the keywords “skin” and “hair”. Article retrieval was conducted via the Web of Science database using an in-house Python script (https://github.com/jpanzhang/WOS.scrape). Candidate genes from the genome-wide association analysis were compared with DEGs identified through mRNA-seq analysis of high- and low-CHD skin samples. A Venn diagram was generated to identify overlapping genes between the genome- and transcriptome-level findings.

Multi-tissue gene expression profiling

To assess tissue specificity, a total of 138 mRNA-seq samples (heart, *n*=13; liver, *n*=20; spleen, *n*=13; lung, *n*=22; kidney, *n*=20; muscle, *n*=34; and skin, *n*=16) were downloaded from five publicly available datasets: PRJEB42490 (https://data.faang.org/home), PRJEB23196 (Muriuki et al., 2019), PRJNA160149 (Dong et al., 2013), PRJNA309284 (Tang et al., 2017), and PRJNA276799 (Tang et al., 2017). Read alignment and gene quantitation were performed using the same pipeline as described previously. The resulting FPKM matrix of 138 samples (Supplementary Table S2) was used to assess the enrichment of candidate gene expression in skin tissue.

Western blotting

Western blotting was conducted to quantify the protein expression of GJA1 and GPRC5D in skin samples from goats in the high-CHD (*n*=3) and low-CHD (*n*=3) groups. Protein extraction, electrophoresis, and antibody incubation were performed as described in previous research (Li et al., 2020). Primary antibodies against GJA1, GPRC5D, and ACTB (Bioworld Technology, USA) were used. Hybridizing bands were visualized using the SuperSignal West Pico Chemiluminescent Substrate kit (ThermoFisher, USA) and captured with the SH-523 chemiluminescence imaging system (SHST, China). ImageJ software (http://imagej.net/ImageJ) was used for grayscale quantification, and independent-sample *t*-tests were used to compare protein expression between the high- and low-CHD groups.

Immunohistochemical staining

To localize GJA1 and GPRC5D protein expression within the skin, immunohistochemical (IHC) staining was performed on paraffin-embedded skin sections from six goats (*n*=3 per high- and low-CHD group). The antibodies used were identical to those applied in western blot analysis. Tissue processing included fixation, gradient dehydration, paraffin embedding, sectioning, antigen retrieval, blocking, primary and secondary antibody incubation, hematoxylin counterstaining, and slide mounting. Slides were scanned using a Pannoramic DESK digital scanner (3D HISTECH, Hungary). Hematoxylin-stained areas were removed using the IHC toolbox plugin in ImageJ to isolate 3,3'-diaminobenzidine (DAB)-positive staining, indicating locations of the target protein. The IHC staining signal was quantified by calculating the average optical density (AOD) for each sample, and differences between the high- and low-CHD groups were assessed using an independent-sample *t*-test.

Gene expression profile of *GJA1* and *GPRC5D* in skin cell types

Single-cell RNA sequencing enables transcriptome profiling at single-cell resolution, allowing precise identification of gene expression across diverse cell populations. To identify the specific cell types expressing *GJA1* and *GPRC5D*, skin single-cell transcriptome data from two adult Liaoning cashmere goats were obtained from PRJNA756314 (Wang et al., 2021). Methodological details, including single-cell isolation, library construction, sequencing, alignment to the reference genome, data normalization, and cell-type annotation, are described in the original publication (Wang et al., 2021). The expression profiles of *GJA1* and *GPRC5D* were examined across all skin cell types.

Gene expression profile of *GJA1* and *GPRC5D* under different hair follicle densities

To assess whether *GJA1* and *GPRC5D* expression levels respond to changes in hair follicle density, transcriptome profiling was conducted using skin samples from body sites with known differences in follicle density. Based on the reported inhomogeneous distribution of hair follicle density in goats (Zhang et al., 2020a), skin transcriptome sequencing was performed on different body sites (forearm and inner side of forearm) of three Inner Mongolia cashmere goats and three Dazu black goats. These samples, collected during the winter catagen phase of secondary hair follicles, are available under PRJNA1212483 (Zhang et al., 2025a). Read mapping and gene quantification were performed following the established pipeline. The resulting FPKM matrix from 12 skin samples was analyzed to determine differential expression of candidate genes across body sites with varying hair follicle densities.

To examine expression variation across breeds with differing hair follicle density, skin transcriptome sequencing was also performed on four Chinese goat breeds, including Inner Mongolia cashmere goats (*n*=3), Dazu black goats (*n*=3), Banjiao goats (*n*=3), and Yudong black goats (*n*=3). All samples were collected from the lateral chest (site #6) during the catagen phase. This dataset, currently unpublished, is accessible under PRJNA1252663. Standard read mapping and gene quantification were performed. This resulting FPKM matrix of 12 skin samples was used to compare gene expression patterns of *GJA1* and *GPRC5D* across breeds with varying follicle densities.

Additional mRNA-seq samples were included to further compare expression between cashmere-producing and non-cashmere goats. mRNA-seq data from Shanbei cashmere goats (*n*=5) and Chuannan black goats (*n*=5) were obtained from CNP0003532 (Wang et al., 2023) (China National GeneBank Database), while Inner Mongolia cashmere goats (*n*=4) and Sasnen dairy goats (*n*=4) were obtained from PRJNA335792 (NCBI) (Zhang et al., 2019). Read mapping and gene quantification were performed as previously described. The resulting FPKM matrices were used to evaluate differential expression of the candidate genes across goat breeds with contrasting hair follicle phenotypes.

RESULTS

CHD decreases with body growth

The goat trunk was approximated as an elliptical cylinder (Figure 2A), supported by a strong correlation between actual CG and ThCG (R=0.97, *P*=2.5e-37, Supplementary Figure

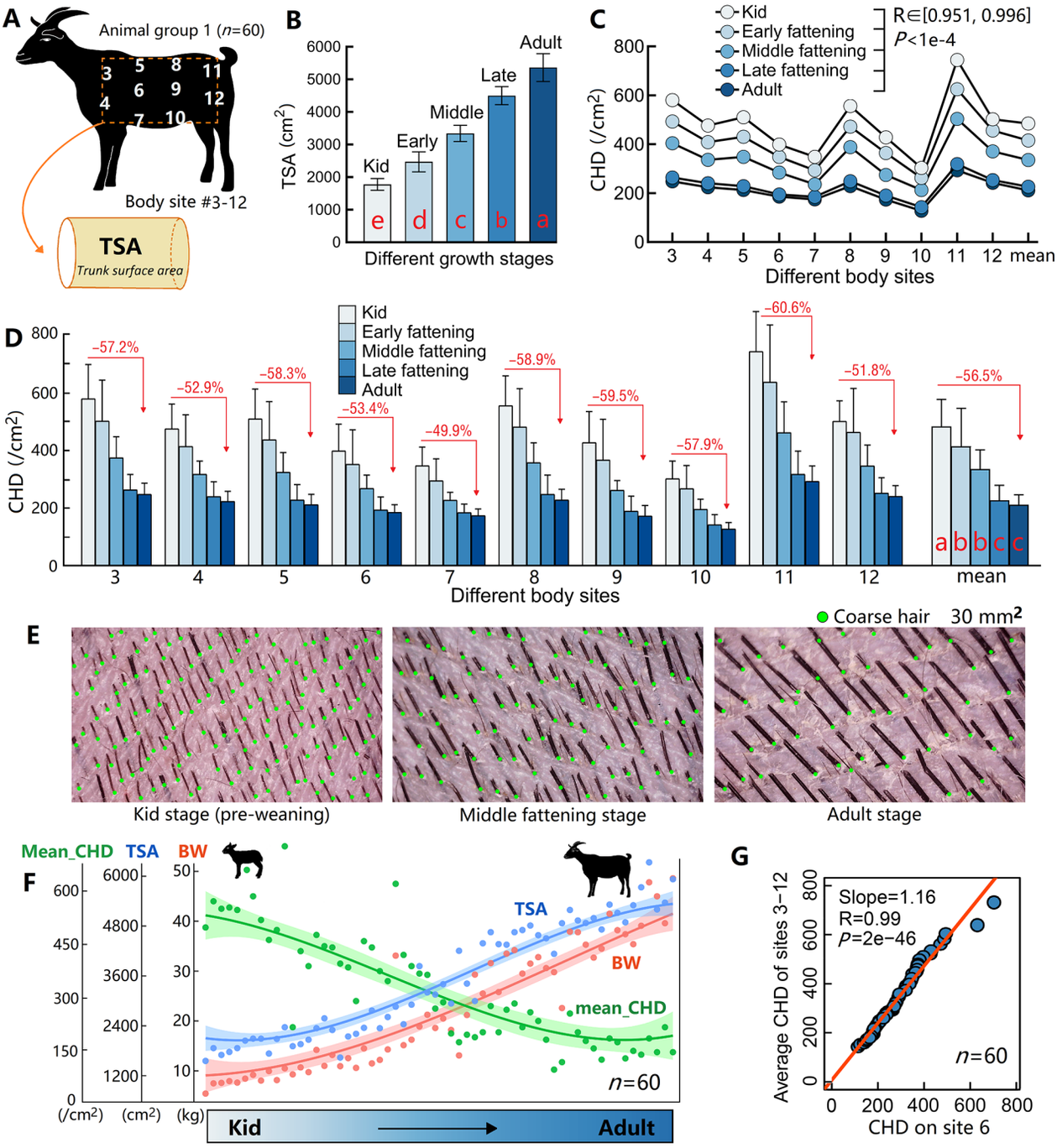

Figure 2 Spatiotemporal patterns of CHD

A: Goat trunk was approximated as an elliptical cylinder to enable calculation of TSA. B: TSA increased progressively with body growth. C: CHD distribution patterns across the 10 body sites remained consistent from kid to adult stages. D: CHD declined by more than 50% at all sites from kid to adult stages. E: Representative 30 mm^2 skin images from Dazu black goats at kid, mid-fattening, and adult stages. F: Relationships among BW, TSA, and mean_CHD. BW increased with age, accompanied by TSA expansion and a corresponding decrease in mean_CHD, calculated as the arithmetic mean across sites #3 to #12. G: CHD at site #6 showed a near-perfect correlation with the average CHD across sites #3 to #12, supporting its use as a representative site for further analysis. Results are presented as mean±SD. Different lowercase letters indicate significant statistical differences (P<0.05). CHD, coarse hair density; TSA, trunk surface area; BW, body weight.

S4). ThCG was derived from the circumference of a theoretical ellipse calculated using CD and CW, with BL, CD, and CW representing the long axis, long diameter, and short diameter, respectively. No significant sex-based differences in CHD were observed (Supplementary Figure S5); therefore, subsequent analyses were conducted without regard to sex.

TSA increased progressively with body growth, with mean values of 1 775.1±181.4, 2 470.8±307.1, 3 344.0±274.6, 4 499.9±274.6, and 5 361.8±424.2 cm^2 across the five growth stages, respectively (Figure 2B). CHD exhibited non-uniform distribution across body sites, although this spatial heterogeneity declined with maturation (Figure 2C). Across all stages, CHD at site #11 was consistently the highest, significantly exceeding other sites (P<0.05), whereas site #10

showed the lowest values (Supplementary Table S3). Distribution patterns remained stable across growth stages, with Pearson correlation coefficients ranging from 0.951 to 0.996 (*P*<1e-4, Figure 2C). Interestingly, CHD declined by approximately 50%–60% at each body site during development, indicating consistency of CHD changes across the whole body (Figure 2D), yet the estimated total number of coarse hairs (TSA×CHD) remained relatively stable at approximately 1 000 000 across all growth stages (Supplementary Figure S6), suggesting a trade-off between body expansion and follicle density.

Representative skin surface images at three developmental stages illustrated that hair shafts thickened while becoming less dense with age (Figure 2E). BW, TSA, and CHD trajectories showed that as goats matured, BW and surface area increased, while CHD progressively declined (Figure 2F). In adulthood, all three traits plateaued, supporting the use of adult animals for subsequent molecular analyses to minimize confounding from developmental variation. CHD at site #6 showed a near-perfect correlation with mean CHD across sites #3–12 (R=0.99, *P*=2e-46; Figure 2G), validating its selection as a representative site for the subsequent transcriptomic and genomic studies.

Transcriptome-based identification of CHD-associated genes

Based on measured CHD values, the 33 skin samples were categorized into low-, med-, and high-CHD groups, with mean CHD values of 211.0±21.8, 254.5±14.0, and 292.8±9.6 coarse hairs/cm^2 (Figure 3A, B), respectively. mRNA-seq yielded 200.4 Gb of raw data (Supplementary Table S4), which, following quality control, read mapping, transcript assembly, and quantification, produced a normalized FPKM matrix (Supplementary Table S5). PCA (Figure 3C) and hierarchical clustering (Figure 3D) revealed greater repeatability among the intra-group samples compared to the inter-group samples. Differential expression analysis using incremental replicate subsets (*n*=6 to 11 per group) identified 1 724 up-regulated and 580 down-regulated genes that were stably differentially expressed (Figure 3E; Supplementary Table S6). To validate transcriptomic findings, 29 DEGs were randomly selected for qPCR analysis (Supplementary Table S7). All primer pairs exhibited high amplification efficiency and specificity (Supplementary Figure S7). Of the 29 genes, 25 exhibited significantly elevated expression in the high-CHD group (*P*<0.05; Supplementary Figure S8). A strong correlation was observed between the qPCR and mRNA-seq results (R=0.88, *P*=2.8e-10), confirming the reliability of the identified DEG dataset (Figure 3F).

To further identify CHD-related gene networks, WGCNA was performed on the same 33 samples. Two gene co-expression modules, “magenta” and “darkgreen”, comprising 986 and 148 genes, respectively, exhibited the strongest associations with CHD, with correlation coefficients of −0.7 (*P*=6.6e-6) and 0.66 (*P*=2.9e-5) (Figure 3G; Supplementary Table S8). A total of 572 genes overlapped between the DEGs and WGCNA modules, highlighting potential candidates (Figure 3H; Supplementary Table S9).

Genomic variant summary and population structure

Among the 272 adult goats analyzed, CHD and CHD_norm values followed approximately normal distributions, ranging from 86.7 to 440.0 and 84.1 to 351.9 coarse hairs/cm^2, respectively (Figure 4A; Table 1; Supplementary Table S10). A weak but statistically significant correlation was observed between TSA and CHD (R=0.17, *P*<0.01, Figure 4B), indicating that TSA correction may have limited utility for CHD normalization in adults. Whole-genome sequencing generated 4 800.0 Gb of data (Supplementary Table S11), with each individual contributing approximately 117.6 million reads at an average sequencing depth of 6×. Quality metrics were high, with mean Q20 (sequencing error rate <1%) and Q30 (sequencing error rate <0.1%) values exceeding 96% and 91%, respectively.

After stringent quality control, mapping, variant calling, and filtering, 11 025 802 SNPs were retained for subsequent analyses (Figure 4C). PCA showed that the top two PCs accounted for 11.8% of total variance and revealed mild population stratification (Figure 4D). Pairwise relatedness coefficients were mostly centered between −0.05 and 0.05 (Supplementary Figure S9), indicating low genetic relatedness within the sampled population. These results demonstrated that PCs and genetic relatedness should be considered for subsequent GWAS models.

CHD-associated genes identified by GWAS

Genome-wide association analysis was conducted using a LMM incorporating the top 20 PCs and the kinship matrix. The QQ plot revealed a genomic inflation factor between 0.98 and 1.02, confirming that the GWAS model was reliable. GWAS for CHD identified 23 SNPs surpassing the genome-wide significance threshold (Figure 4E; Supplementary Table S12), 15 of which were located within the chr9.15931585-18621011 region. Notably, six of the 23 significant SNPs were also identified in the GWAS of CHD_norm (Figure 4F). Individuals carrying certain alleles at these significant SNPs exhibited higher CHD values (*P*<9.07e-8) (Figure 4G). A total of 48 genes were located within ±500 kb of the lead SNPs (Figure 4H; Supplementary Table S13). Among these, six genes (*CD1D*, *GJA1*, *GPRC5D*, *CD207*, *TFAM*, and *CXCL12*) were associated with “skin” or “hair” based on literature mining (Figure 4I). Venn diagram analysis was conducted on the genes identified by GWAS and mRNA-seq, with three genes (*ATP6V1B1*, *GJA1*, and *GPRC5D*) found to overlap (Figure 4J).

***GJA1* and *GPRC5D* are highly and specifically expressed in skin tissue**

To evaluate tissue specificity, the expression profiles of the seven candidate genes (*CD1D*, *ATP6V1B1*, *CD207*, *TFAM*, *CXCL12*, *GJA1*, and *GPRC5D*) were assessed across seven tissue types (Supplementary Table S14). Interestingly, only *GJA1* and *GPRC5D* were highly (FPKM > 50) and specifically expressed in skin tissue (Figure 5A). Although *CD207* also exhibited skin-specific expression, its overall expression was low, potentially limiting its relevance to follicular function. These data support a prominent role for *GJA1* and *GPRC5D* in skin biology.

***GJA1* and *GPRC5D* are strongly associated with CHD**

Genomic mapping showed that *GJA1* was located within the key genomic region of chr9.15931585-18621011, while *GPRC5D* was positioned approximately 500 kb from significant SNPs including chr5_95957684 and chr5_96041799 (Figure 5B, C). No significant SNPs were located directly within either gene, suggesting two possible scenarios: (1) significant SNPs may exert remote *cis*-regulatory effects on *GJA1* and *GPRC5D* expression, or (2)

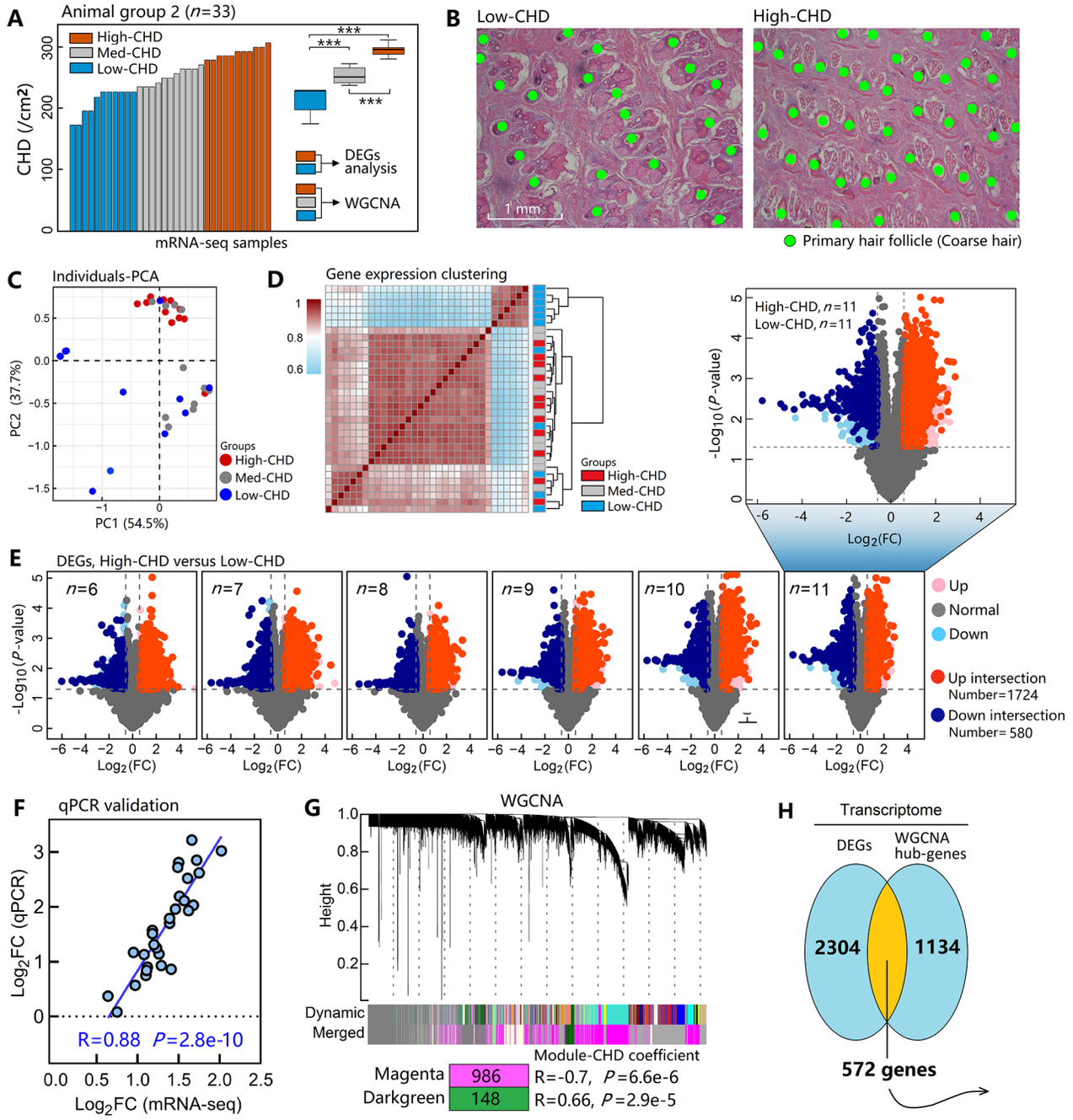

Figure 3 Identification of core genes associated with CHD through transcriptomic analysis

A: Thirty-three skin samples were categorized into high-, med-, and low-CHD groups based on their measured CHD values. DEG analysis was conducted between the high- and low-CHD groups, and WGCNA was performed on all samples. B: Representative histological images from high- and low-CHD samples illustrating follicle morphology differences. C: PCA plot illustrating that inter-group variance exceeded intra-group variance. D: Heatmap showing gene expression profiles across 33 samples, showing distinct clustering by CHD group. E: Serial volcano plots of DEGs identified from comparisons between high- and low-CHD groups. A total of 1 724 up-regulated and 580 down-regulated DEGs overlapped across all comparisons (sample sizes 6–11). F: Comparison of fold changes for 29 target genes identified by mRNA-seq and qPCR. G: WGCNA identified two significant gene modules containing 1 134 hub genes associated with CHD. H: Venn diagram showing 572 overlapping genes identified by both DEG and WGCNA approaches. ***: P<0.001. CHD, coarse hair density; DEG, differentially expressed genes; PCA, principal component analysis; WGCNA, weighted gene co-expression network analysis.

true causative variants may lie below the genomic detection threshold. In any case, integrated genomic and transcriptomic analysis revealed that both *GJA1* and *GPRC5D* were skin-specific (Figure 5A), differentially expressed between high- and low-CHD groups (Figure 5D), and exhibited the strongest expression correlation with CHD among all candidates (Figure 5E). Additionally, a robust positive correlation between *GJA1* and *GPRC5D* expression (R=0.90, P<0.001, Figure 5E) suggested potential functional synergy between these genes.

Localization of *GJA1* and *GPRC5D* and their proteins

Semi-quantitative statistics for western blot assays revealed that GJA1 protein levels differed significantly between high- and low-CHD individuals (P=0.02, Figure 6A, B), while the

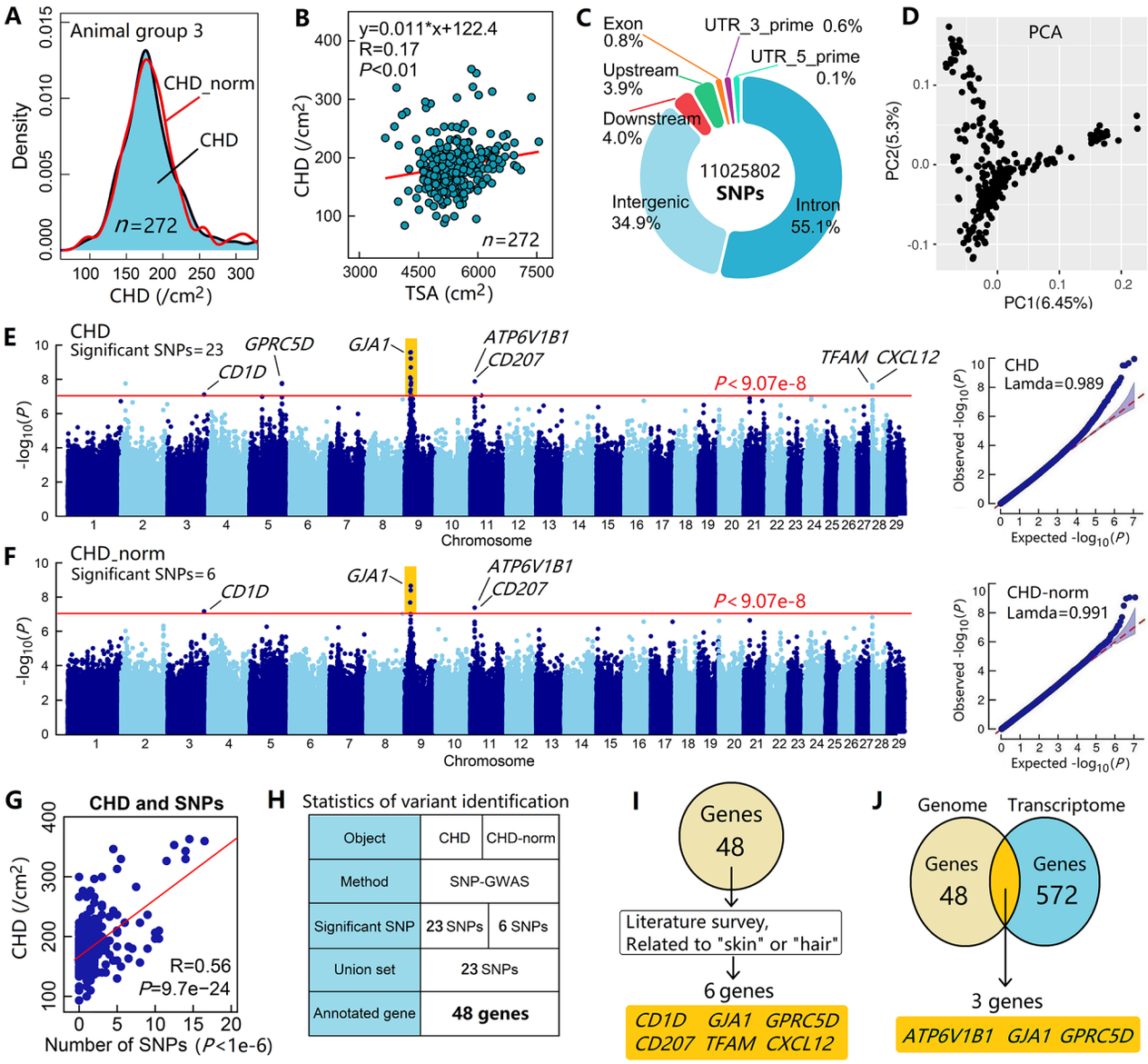

Figure 4 Significant genomic variants and candidate genes associated with CHD

A: CHD and CHD_norm values in 272 goats followed an approximately normal distribution. B: TSA and CHD exhibited a weak correlation in adult goats. C: Functional classification and genomic location distribution of identified SNPs. D: PCA plot based on genome-wide variants. E, F: Manhattan plots and QQ plots for GWAS of CHD (E) and CHD_norm (F). G: CHD values changed with the number of SNPs exceeding genome-wide threshold (*P*=1e-6). H: Twenty-five significant SNPs were annotated to 48 genes within ±500 kb. I: Literature review identified six genes associated with “skin” or “hair”. J: Venn diagram showing three overlapping genes between genomic and transcriptomic results. CHD, coarse hair density; CHD_norm, CHD value normalized by TSA value; TSA, trunk surface area.

GPRC5D protein exhibited a similar trend without reaching statistical significance (*P*=0.22, Figure 6A, B). IHC staining of transverse skin sections showed that the GJA1 protein was widely expressed, with strong localization in both primary and secondary hair follicle clusters as well as sebaceous glands (Figure 6C). In contrast, GPRC5D was primarily localized around secondary hair follicles (Figure 6D). Comparisons of the two proteins at the same locations revealed that the GJA1 protein exhibited more abundant and widespread expression (Supplementary Figure S10). AOD was measured within a 5 mm² region for each sample, and independent sample *t*-tests were conducted to evaluate CHD group differences. The GJA1 protein showed significant differential expression (Figure 6E), whereas GPRC5D showed a similar pattern but without statistical significance (Figure 6F). These protein-level findings were consistent with the transcriptomic results.

Single-cell transcriptomic analysis of two skin samples yielded 13 051 high-quality cells, primarily annotated into 13 distinct cell types. An anatomical overview of skin structure and the spatial distribution of cell types is presented in Figure 6G. Notably, *GJA1* transcription was predominantly detected in hair follicle stem cells and dermal papilla cells, while *GPRC5D* was primarily transcribed in dermal papilla cells (Figure 6H). These two cell populations are central to hair follicle regeneration and growth through self-renewal and differentiation. Complementary IHC staining further demonstrated that both proteins were translated around hair follicles, particularly in regions enriched with hair follicle stem cells as well as inner and outer root sheath cells (Figure 6H). Together, the single-cell transcriptomic and IHC results

Table 1 Descriptive statistics of CHD and TSA traits in 272 adult goats

Trait	Unit	Mean	Coefficient variation (%)	Sample size (*n*)
TSA	cm^2	5 421.0	11.5	272
CHD	coarse hairs/cm^2	187.4	25.7	272
CHD_norm	coarse hairs/cm^2	185.5	23.0	272

TSA, trunk surface area; CHD, coarse hair density; CHD_norm, CHD value normalized by its TSA value.

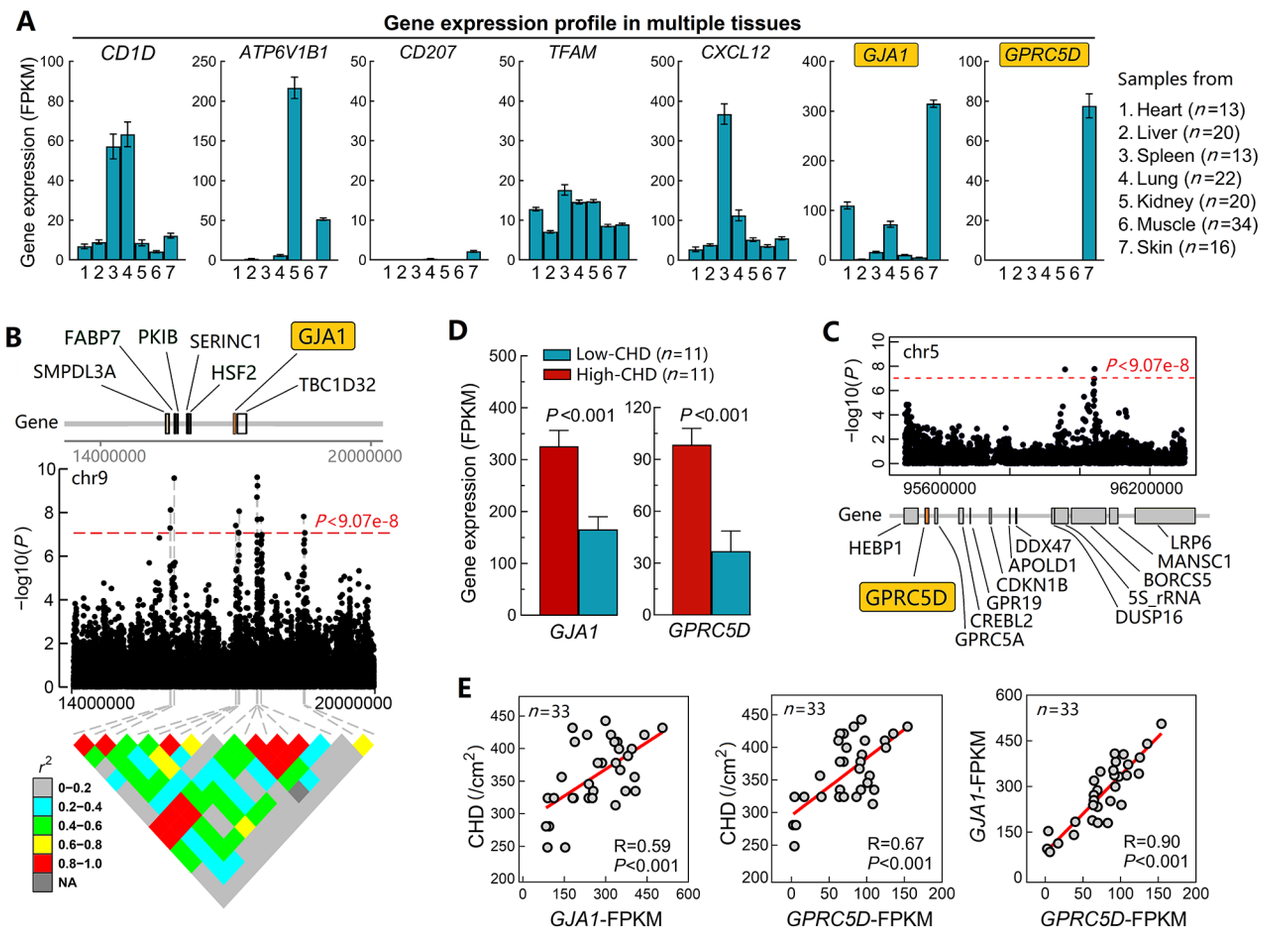

Figure 5 *GJA1* and *GPRC5D* are highly and specifically expressed in skin tissue

A: Expression profiles of seven genes in heart, liver, spleen, lung, kidney, muscle, and skin tissues. Only *GJA1* and *GPRC5D* showed high and specific expression in skin tissue. B: Gene distribution and local Manhattan plot showing localization of *GJA1* in chr9.15931585-18621011 region. C: *GPRC5D* is located 385 kb from the nearest genome-wide significant SNP, chr5_95957684. D: Expression levels of *GJA1* and *GPRC5D* in high- and low-CHD groups. E: Correlation scatter plots between *GJA1* and *GPRC5D* expression levels and CHD. CHD, coarse hair density.

elucidated the primary cell types in which *GJA1* and *GPRC5D* function, highlighting hair follicle stem cells and dermal papilla cells as primary candidates for future mechanistic investigations of *GJA1* and *GPRC5D*.

GJA1 and *GPRC5D* respond to changes in hair follicle density

Although this study focused on coarse hair density, the trait also strongly reflects the underlying hair follicle density. To examine whether *GJA1* and *GPRC5D* respond to changes in follicle density, transcriptomic data from distinct body sites were analyzed in Inner Mongolia cashmere goats and Dazu black goats (Figure 7A). Significant differences in follicle density were observed between the forearm and inner forearm in both breeds ($P<0.01$, paired-sample *t*-test; Figure 7B). Surprisingly, *GJA1* expression was highly consistent with hair follicle density across both body sites and breeds (Figure 7C). *GPRC5D* expression levels showed a similar trend within breeds, although the differences were not significant (Figure 7D).

Histological comparisons across breeds further demonstrated that cashmere goats consistently exhibited higher hair follicle density than non-cashmere goat breeds ($P<0.01$, Figure 7E, F). Correspondingly, *GJA1* expression was significantly elevated in the skin of cashmere goats relative to each non-cashmere breed ($P<0.05$, Figure 7G). In contrast, *GPRC5D* expression displayed inconsistent correlations with hair follicle density across breeds (Figure 7H), including divergent trends between Inner Mongolia cashmere goats and Dazu black goats (Figure 7D versus Figure 7H), suggesting lower stability of this marker across genetic backgrounds.

To further investigate these associations, transcriptome data from two additional independent datasets were analyzed.

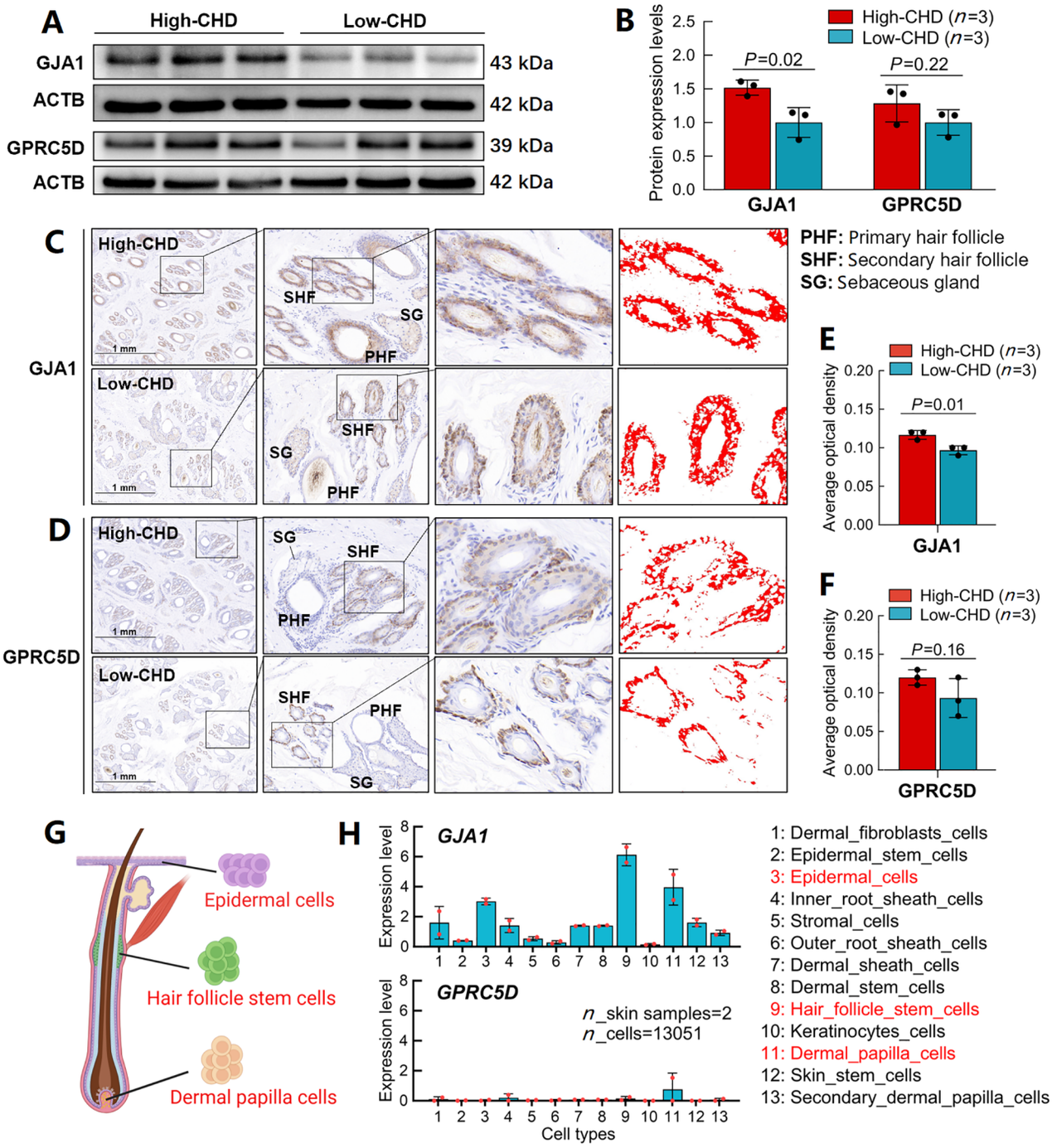

Figure 6 Protein expression and single-cell gene expression profiles

A: Western blot bands of three proteins in the high- and low-CHD groups. B: Relative expression levels of GJA1 and GPRC5D proteins. C: Immunohistochemical localization of GJA1 protein, predominantly expressed in both primary and secondary hair follicles, as well as sebaceous glands. D: Immunohistochemical localization of GPRC5D protein, primarily expressed in secondary hair follicles with minimal expression in primary hair follicles and sebaceous glands. Red regions in C and D represent DAB-positive areas, indicating locations of target protein. E: Quantification of GJA1 protein expression between high- and low-CHD samples (n=3 for each), showing significant differences. F: GPRC5D protein expression showed a trend consistent with hair density but was not significant. G: Schematic illustration of hair follicle structure and associated cell types. H: Single-cell expression profiles showing that *GJA1* and *GPRC5D* were predominantly expressed in hair follicle stem cells and dermal papilla cells. Both IHC and single-cell transcriptomic analysis supported that that GJA1 and GPRC5D were localized within hair follicle structures. CHD, coarse hair density.

In the comparison between Shanbei white cashmere goats and Chuannan black goats, both *GJA1* and *GPRC5D* were significantly up-regulated in the cashmere goats (P<0.05; Figure 7I, J). In the comparison between Inner Mongolia cashmere goats and Saanen dairy goats, *GJA1* again exhibited significantly higher expression in the cashmere goats, while *GPRC5D* presented a similar trend without statistical significance (Figure 7K, L).

Across all four datasets, *GJA1* consistently demonstrated strong and significant concordance with variations in hair

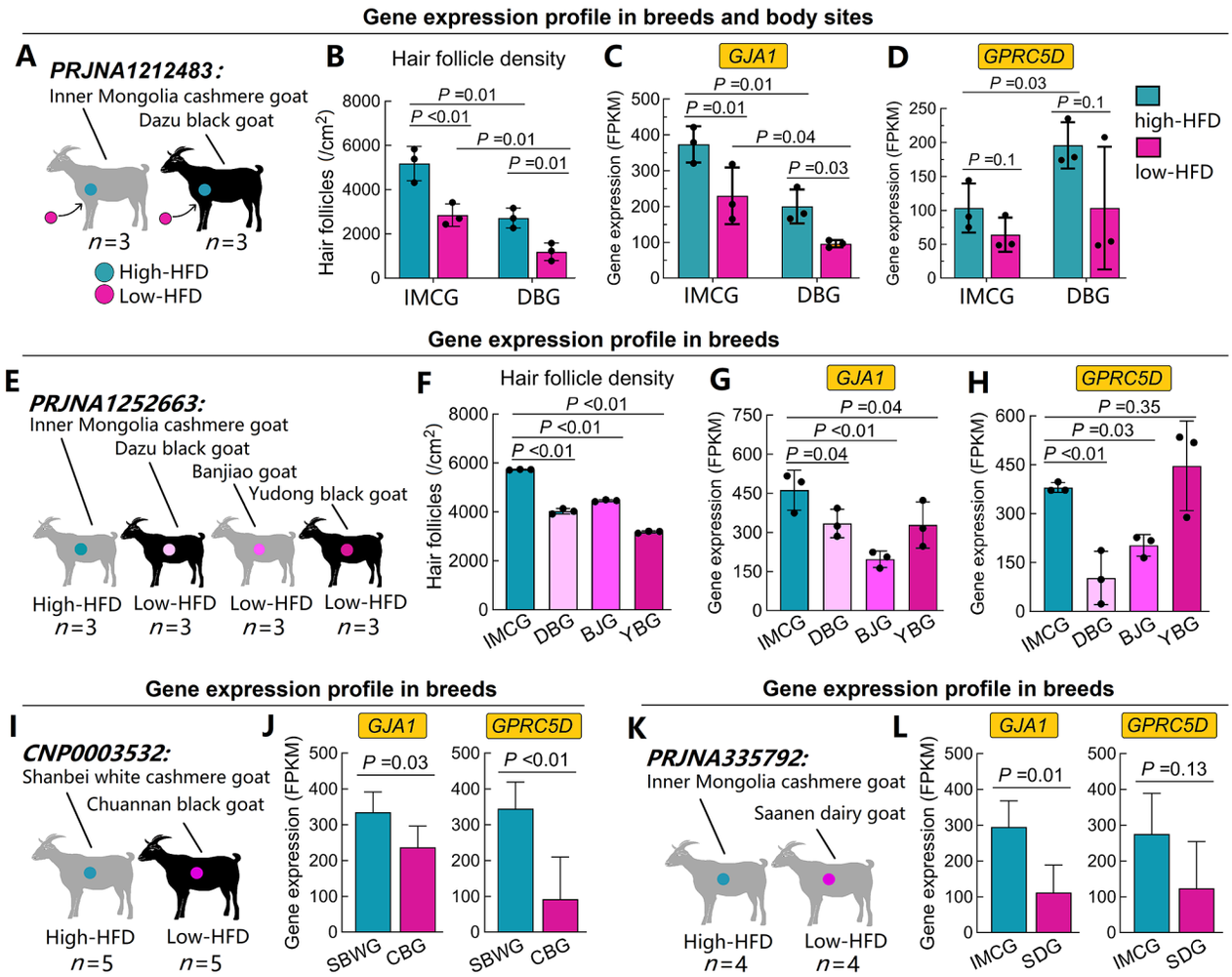

Figure 7 Differential expression of *GJA1* and *GPRC5D* across body sites and breeds

A, B: To investigate variation in hair follicle density (HFD) across body sites, skin transcriptome sequencing was conducted on 12 samples from the forearm and inner forearm of goats. C, D: Expression profiles of *GJA1* and *GPRC5D* in different body sites. E: Transcriptomic data from 12 skin samples collected from four goat breeds. F: Cashmere goats exhibited significantly higher HFD compared to non-cashmere goats. G, H: Expression profiles of *GJA1* and *GPRC5D* across four goat breeds. I, J: Comparative expression of *GJA1* and *GPRC5D* between SBWG and CBG. K, L: Comparative expression of *GJA1* and *GPRC5D* between IMCG and SDG. IMCG, Inner Mongolia cashmere goat; DBG, Dazu black goat; BJG, Banjiao goat; YDG, Yudong goat; SBWG, Shanbei white cashmere goat; CBG, Chuannan black goat; SDG, Saanen dairy goat; HFD, hair follicle density.

follicle density. In contrast, *GPRC5D* showed more variable expression patterns, especially in inter-breed comparisons. While several comparisons for *GPRC5D* did not reach statistical significance, this may reflect limited sample sizes. Overall, these cross-project analyses provide strong support for the potential involvement of *GJA1* and *GPRC5D* in the regulation of hair and follicle density in goats.

Comprehensive evaluation of candidate genes

Candidate genes were evaluated based on multidimensional assessment incorporating genomic association signals, transcript abundance and specificity, protein expression profiles, and literature support. As shown in Table 2, *GJA1* and *GPRC5D* emerged as the most compelling candidates associated with hair density and hair follicle density, supported by the following lines of evidence: (1) both genes were annotated by GWAS; (2) they exhibited consistent differential expression between high- and low-CHD individuals in Dazu black goats; (3) existing literature has implicated their involvement in skin and hair biology; (4) they were highly expressed (FPKM>50) and specifically enriched in skin tissue; (5) their protein levels differed between CHD groups; (6) protein localization was concentrated within hair follicles; (7) transcriptomic and protein evidence indicated functional relevance in major follicular cell types; (8) expression levels varied with hair follicle density across anatomical sites; and (9) both genes were differentially expressed between cashmere and non-cashmere goat breeds.

DISCUSSION

Through the innovative application of micro-camera technology for high-throughput assessment of coarse hair density in Dazu black goats, combined with transcriptomic and genomic data, this study identified *GJA1* and *GPRC5D* as robust candidate genes associated with hair density. These findings address a significant knowledge gap regarding the spatiotemporal characteristics and molecular determinants of mammalian hair and follicle density.

Previous research has largely focused on fiber length (Li

Table 2 Comprehensive valuation of seven candidate genes

Item of evidence	Source	*CD1D*	*ATP6V1B1*	*CD207*	*TFAM*	*CXCL12*	*GJA1*	*GPRC5D*
1. Gene located near significant SNPs associated with CHD	Genome-wide association study	Yes	Yes	Yes	Yes	Yes	Yes	Yes
2. Stable DEG between high- and low-CHD groups	Skin transcriptome	No	Yes	No	No	No	Yes	Yes
3. Supporting literature related to skin or hair biology	Literature survey	Yes	No	Yes	Yes	Yes	Yes	Yes
4. Highly and specifically expressed in skin tissue	Multi-tissue transcriptome	–	–	–	–	–	Yes	Yes
5. Protein showed significant differences between high- and low-CHD groups	West blotting and immunohistochemistry	–	–	–	–	–	Yes	No
6. Protein densely present around hair follicles	Immunohistochemistry	–	–	–	–	–	Yes	Yes
7. Acted on hair follicles through hair follicle stem cells or dermal papilla cells	Skin single-cell transcriptome	–	–	–	–	–	Yes	Yes
8. Differential expression across different body sites in response to HFD changes	Skin transcriptome of multi-sites	–	–	–	–	–	Yes	Yes
9. Differential expression across different goat breeds in response to HFD changes	Skin transcriptome of multi-breeds	–	–	–	–	–	Yes	Yes (unstable)
Overall							Strong candidate gene	Strong candidate gene

Only *GJA1* and *GPRC5D* were investigated in items 5–9, as other genes had been filtered out in items 1–4. "Yes" indicates that gene met the corresponding criteria, while "No" indicates that it did not; "–" indicates that gene was not tested. CHD, coarse hair density; HFD, hair follicle density; DEG, differentially expressed genes.

et al., 2017; Zhao et al., 2018) and fineness (Wang et al., 2021; Zhang et al., 2025b), with fiber density receiving comparatively little attention, primarily due to limitations in measurement methodologies. The traditional technique—manually counting fibers per unit area (Ministry of Agriculture and Rural Affairs of the People's Republic of China, 2010) —is prone to substantial error. Histological section analysis, although more accurate, is labor-intensive and requires complex sample processing (Nixon, 1993). These challenges have hindered progress in identifying genes regulating hair density and their application in selective breeding programs. The present study overcame these limitations through the innovative use of micro-camera imaging, enabling efficient large-scale phenotyping. Our previous study (Zhang et al., 2022a) demonstrated that a 5 mm² sampling area is statistically sufficient for estimating follicle density. Thus, the 30 mm^2 field of view captured by the micro-camera in this study provided high statistical power for CHD determination. While this approach may be unsuitable for cashmere goats and Merino sheep due to their high fiber density and low contrast between hair and skin, it proved highly effective in Dazu black goats, whose coarse black hairs offer strong visual separation for micro-camera imaging. The selection of both imaging technology and animal model reflects a strategic match between phenotyping tool and biological system.

While several studies have focused on the recognition of animal fibers, such as wool and cashmere, these efforts have primarily emphasized classification techniques using neural networks and image analysis. For example, (Zhong et al., 2017) developed a neural network-based classification method using fiber images captured through optical microscopy. (Xing et al., 2019) introduced a cashmere identification approach based on a gray-level co-occurrence matrix, interactive measurement, and K-means clustering. (Zang et al., 2022) applied multi-scale geometric analysis combined with deep convolutional neural networks to distinguish between cashmere and guard hairs. In contrast, studies on hair density have been largely confined to human dermatology. (Urban et al., 2021) trained convolutional neural networks on 70 optical coherence tomography images and achieved rapid image acquisition (3 s) and automated follicle counting (1 s). (Gao et al., 2022; Urban et al., 2021) developed a deep learning model using 2 910 hair follicular images that accurately quantified hair density and diameter in human hair images. However, fundamental differences in fiber type and density between humans and fur-bearing animals limit the applicability of these algorithms for animals. Therefore, it is imperative to develop automated techniques for hair density determination that can be tailored to the anatomical and physiological characteristics of fur- and fiber-producing animals.

Although the temporal dynamics of hair follicle development during embryogenesis, postnatal maturation, and seasonal cycling have been extensively studied (Wu et al., 2023; Zhang et al., 2018), few studies have examined the changes in hair density from a whole-body perspective. In this study, large-scale imaging across multiple anatomical sites revealed a progressive decline in hair density with increasing body size. Since most hair follicles are established *in utero* and the follicle reserve is primarily determined by birth, early developmental stages, particularly the embryonic period and first six months, are critical factors determining hair density in adult goats (Diao et al., 2023). While direct longitudinal evidence is lacking, the hypothesis that total postnatal hair count remains constant is partially supported by our estimates of total trunk hairs across developmental stages. However, the absence of long-term tracking within the same individuals limits the strength of this conclusion. Assuming relative constancy in total hair number, the observed decline in CHD can be attributed to surface area expansion during growth. This finding offers valuable insight into the morphological basis of density changes. To eliminate confounding effects from developmental stage, only adult goats were included in the genomic and transcriptomic analyses.

The primary objective of identifying candidate genes associated with hair density is to facilitate their application in molecular breeding programs aimed at improving fiber yield. Our previous study showed that maximum hair follicle density in Inner Mongolia cashmere goats could reach up to 1.5 times current levels (Zhang et al., 2022b), indicating substantial untapped breeding potential. Additionally, higher hair density

is often correlated with finer fiber diameter, a pattern observed in multiple fur- and fiber-producing species, such as goats (Zhang et al., 2022b), sheep (Scobie & Young, 2000), and Huacaya alpacas (Ferguson et al., 2012; Moore et al., 2015). These findings suggest that increasing fiber density not only enhances yield but also improves fiber quality, making it a key target for genetic improvement in fur-producing animals. Despite the clear benefits of increasing hair density, research into the genetic determinants of hair density remains limited.

Several genes have been reported to influence hair follicle density across species, including *En1* (Kamberov et al., 2015), *DKK2* (Song et al., 2018), and *BMP6* (Wu et al., 2019) in mice, *MAP2* in pigs (Jiang et al., 2019), *EDAR* in sheep (Liang et al., 2024), and *WNT4* in rabbits (Yang et al., 2023). Notably, *En1* expression in mouse footpads significantly affects hair follicle distribution (Kamberov et al., 2015), while *DKK2* expression regulates hairless phenotypes in mouse planter skin (Song et al., 2018). In fine-wool sheep, SNP mutations in *EDAR* are associated with denser wool production (Liang et al., 2024), while elevated expression levels of *WNT4*, *WNT10a*, and *WNT10b* are associated with increased hair density in rabbits (Yang et al., 2023). Although these studies have provided valuable insights into the genetic basis of hair density, direct evidence linking these target genes to hair density on the main body surface—particularly the lateral trunk side—of economically important animals is still lacking.

Through large-scale genomic and transcriptomic sequencing, this study identified *GJA1* and *GPRC5D* as two novel and compelling candidate genes associated with hair density. It is important to note that “hair density” is functionally equivalent to “hair follicle density”, as each hair fiber originates from a follicle, and in the absence of considering inactive hair follicles, this one-to-one relationship is preserved at the skin surface. *GJA1*, a member of the connexin gene family, encodes connexin 43. In humans, mutations in this gene have been linked to erythrokeratodermia variabilis et progressiva, a congenital skin disorder present at birth (Boyden et al., 2015), and to hypotrichosis, a condition characterized by hair loss (Wang et al., 2015). Our team previously identified four genes (including *GJA1*) associated with hair follicle density in goats through the integration of DEG analysis, trend profiling, and WGCNA (Zhang et al., 2025a). Despite distinct differences in sample sources, experimental conditions, and analytical methods, *GJA1* was consistently identified in both studies, highlighting its crucial role in the regulation of hair and follicle density. *GPRC5D* encodes a member of the G-protein coupled receptor family (Family C, Group 5, Member D). Previous studies have reported that *GPRC5D* is exclusively expressed in goat skin (Jin et al., 2014) and plays an important role in hair follicle development (Gao et al., 2016). Although no studies in non-goat species have directly linked these genes to hair or follicle density, associations between *GJA1* and hair loss phenotypes in humans provide indirect support for their functional relevance in follicular biology.

In addition to the literature survey, eight independent lines of evidence strongly supported the potential roles of *GJA1* and *GPRC5D* in hair density regulation, including one genomic-level, five transcriptomic-level, and two protein-level observations (Table 2). Although only one line of evidence originated from GWAS, it was the most influential, identifying 23 genome-wide significant SNPs and rapidly narrowing the candidate pool from over 20 000 genes to a focused set of several dozen. Subsequent filtering through literature review and transcriptome core DEG overlap yielded a refined group of seven candidate genes, effectively reducing the workload for subsequent experimental validation and enhancing research focus. The combined evidence derived from genome-wide variation, transcriptional DEGs, tissue-specific expression profiles, and gene and protein localization, confirmed the critical role of *GJA1* and *GPRC5D* in regulating hair density. These findings fill a longstanding gap in our understanding of genetic factors controlling hair or follicle density in mammals and provide a foundation for future functional and breeding studies.

Hair density, or hair follicle density, is a complex quantitative trait governed by a series of gene networks and signaling pathways. Although this study identified *GJA1* and *GPRC5D* as genes positively correlated with hair density at the genomic, transcriptomic, and protein levels, several limitations should be mentioned. (1) The significant genomic variants identified through GWAS were located several hundred kilobases away from *GJA1* and *GPRC5D*, raising the possibility of long-range *cis*-regulatory effects. However, this study did not include epigenetic modification techniques, which limits the ability to confirm regulatory interactions. (2) The regulatory mechanisms by which *GJA1* and *GPRC5D* influence hair follicle density remain inadequately characterized due to the absence of functional cell biology experiments. Nevertheless, single-cell transcriptomic data identified hair follicle stem cells and dermal papilla cells as critical cell types in which these genes are highly expressed, providing direction for future mechanistic investigations. (3) Comparative studies across mammalian species are notably lacking, and it remains unclear whether the observed associations between *GJA1* and *GPRC5D* and hair density are conserved in other animals. (4) Although this study described spatiotemporal changes in CHD from the kid to adult stages, functional gene identification was performed using samples from adult goats only. The absence of late embryonic and early postnatal skin samples precluded longitudinal validation. Therefore, it is possible that *GJA1* and *GPRC5D* contribute to the maintenance of hair density rather than its initial establishment. Further studies targeting embryonic folliculogenesis are required to clarify the developmental origins of hair density variation.

CONCLUSION

The innovative application of micro-camera imaging enabled large-scale, non-invasive quantification of hair density across the goat body. Hair density exhibited spatial heterogeneity and declined progressively with somatic growth. By integrating genome-wide association analysis, transcriptomic differential expression, and literature evidence, *GJA1* and *GPRC5D* were identified as key genes associated with hair density in goats. Their skin-specific expression, localized primarily to hair follicle stem cells and dermal papilla cells, was positively correlated with changes in hair density. These findings and methodology provide valuable insights for further elucidation of the genetic characteristics and molecular mechanisms underlying hair density in fur- and fiber-producing animals.

DATA AVAILABILITY

The whole-genome sequencing data from 148 goats and skin transcriptome data from 33 goats generated in this study have been deposited in the Sequence Read Archive database (SRA, BioProjectID PRJNA1133099 and PRJNA1133193), Science Data Bank database (SDB, Data DOI:

10.57760/sciencedb.j00139.00230 and 10.57760/sciencedb.j00139.00232), and Genome Sequence Archive database (GSA, CRA026351 and CRA026352).

SUPPLEMENTARY DATA

Supplementary data to this article can be found online.

COMPETING INTERESTS

The authors declare that they have no competing interests.

AUTHORS' CONTRIBUTIONS

J.P.Z. designed the study, collected the samples, analyzed and visualized the data, and drafted the manuscript; M.X. and J.B.F. assisted with image processing; D.L.H. assisted with sample collection; Y.J.Z. supervised the project and revised the manuscript. All authors read and approved the final version of the manuscript.

ACKNOWLEDGMENTS

The authors thank Professor Ze-Ying Wang from the College of Animal Science and Veterinary Medicine of Shenyang Agricultural University for providing the single-cell transcriptome data of two goat skin samples.

REFERENCES

Ansari-Renani HR, Mueller JP, Rischkowsky B, et al. 2012. Cashmere quality of Raeini goats kept by nomads in Iran. *Small Ruminant Research*, **104**(1-3): 10–16.

Bickhart DM, Rosen BD, Koren S, et al. 2017. Single-molecule sequencing and chromatin conformation capture enable *de novo* reference assembly of the domestic goat genome. *Nature Genetics*, **49**(4): 643–650.

Bolger AM, Lohse M, Usadel B. 2014. Trimmomatic: a flexible trimmer for Illumina sequence data. *Bioinformatics*, **30**(15): 2114–2120.

Boyden LM, Craiglow BG, Zhou J, et al. 2015. Dominant *de novo* mutations in *GJA1* cause Erythrokeratodermia variabilis et progressiva, without features of oculodentodigital dysplasia. *Journal of Investigative Dermatology*, **135**(6): 1540–1547.

Chang CC, Chow CC, Tellier LCAM, et al. 2015. Second-generation PLINK: rising to the challenge of larger and richer datasets. *Gigascience*, **4**(1): 7.

Cingolani P, Platts A, Wang LL, et al. 2012. A program for annotating and predicting the effects of single nucleotide polymorphisms, SnpEff: SNPs in the genome of *Drosophila melanogaster* strain w^{1118}; *iso*-2; *iso*-3. *Fly*, **6**(2): 80–92.

Diao XG, Qin JX, Dong CX, et al. 2025. Integrative transcriptomic and metabolomic analyses reveal the role of melatonin in promoting secondary hair follicle development in cashmere goats. *BMC Genomics*, **26**(1): 200.

Diao XG, Yao LY, Duan T, et al. 2023. Melatonin promotes the development of the secondary hair follicles by regulating circMPP5. *Journal of Animal Science and Biotechnology*, **14**(1): 51.

Dobin A, Davis CA, Schlesinger F, et al. 2013. STAR: ultrafast universal RNA-seq aligner. *Bioinformatics*, **29**(1): 15–21.

Dong Y, Xie M, Jiang Y, et al. 2013. Sequencing and automated whole-genome optical mapping of the genome of a domestic goat (*Capra hircus*). *Nature Biotechnology*, **31**(2): 135–141.

Ferguson MB, McGregor BA, Behrendt R. 2012. Relationships between skin follicle characteristics and fibre properties of Suri and Huacaya alpacas and Peppin Merino sheep. *Animal Production Science*, **52**(7): 442–447.

Gao M, Wang Y, Xu HP, et al. 2022. Deep learning-based trichoscopic image analysis and quantitative model for predicting basic and specific classification in male androgenetic alopecia. *Acta Dermato-Venereologica*, **102**: adv00635.

Gao Y, Wang XL, Yan HL, et al. 2016. Comparative transcriptome analysis of fetal skin reveals key genes related to hair follicle morphogenesis in cashmere goats. *PLoS One*, **11**(3): e0151118.

Gu BW, Sun RF, Fang XQ, et al. 2022. Genome-wide association study of body conformation traits by whole genome sequencing in Dazu black goats. *Animals*, **12**(5): 548.

Guan DL, Luo NJ, Tan XS, et al. 2016. Scanning of selection signature provides a glimpse into important economic traits in goats (*Capra hircus*). *Scientific Reports*, **6**(1): 36372.

Hirschhorn JN, Daly MJ. 2005. Genome-wide association studies for common diseases and complex traits. *Nature Reviews Genetics*, **6**(2): 95–108.

Jiang Y, Jiang YF, Zhang HH, et al. 2019. A mutation in MAP2 is associated with prenatal hair follicle density. *The FASEB Journal*, **33**(12): 14479–14490.

Jin M, Li XN, Piao J, et al. 2014. Expression of the GPRC5D gene in Liaoning Cashmere goats. *Turkish Journal of Veterinary & Animal Sciences*, **38**(4): 347–353.

Kamberov YG, Karlsson EK, Kamberova GL, et al. 2015. A genetic basis of variation in eccrine sweat gland and hair follicle density. *Proceedings of the National Academy of Sciences of the United States of America*, **112**(32): 9932–9937.

Li C, Feng C, Ma GY, et al. 2022. Time-course RNA-seq analysis reveals stage-specific and melatonin-triggered gene expression patterns during the hair follicle growth cycle in *Capra hircus*. *BMC Genomics*, **23**(1): 140.

Li H, Durbin R. 2009. Fast and accurate short read alignment with Burrows-Wheeler transform. *Bioinformatics*, **25**(14): 1754–1760.

Li H, Handsaker B, Wysoker A, et al. 2009. The sequence Alignment/Map format and SAMtools. *Bioinformatics*, **25**(16): 2078–2079.

Li JL, Liu LB, Zhang JP, et al. 2020. The expression of miR-129–5p and its target genes in the skin of goats. *Animal Biotechnology*, **32**(5): 573–579.

Li WR, Liu CX, Zhang XM, et al. 2017. CRISPR/Cas9-mediated loss of FGF5 function increases wool staple length in sheep. *The FEBS Journal*, **284**(17): 2764–2773.

Liang BM, Bai TY, Zhao YHT, et al. 2024. Two mutations at *KRT74* and *EDAR* synergistically drive the fine-wool production in Chinese sheep. *Journal of Advanced Research*, **57**: 1–13.

Liu JY, Mu Q, Liu ZH, et al. 2021. Melatonin regulates the periodic growth of cashmere by upregulating the expression of *Wnt10b* and β-*catenin* in Inner Mongolia cashmere goats. *Frontiers in Genetics*, **12**: 665834.

Lu XT, Suo LD, Yan XC, et al. 2024. Genome-wide association analysis of fleece traits in Northwest Xizang white cashmere goat. *Frontiers in Veterinary Science*, **11**: 1409084.

Luigi-Sierra MG, Landi V, Guan DL, et al. 2020. A genome-wide association analysis for body, udder, and leg conformation traits recorded in Murciano-Granadina goats. *Journal of Dairy Science*, **103**(12): 11605–11617.

McCarthy MI, Abecasis GR, Cardon LR, et al. 2008. Genome-wide association studies for complex traits: consensus, uncertainty and challenges. *Nature Reviews Genetics*, **9**(5): 356–369.

McKenna A, Hanna M, Banks E, et al. 2010. The Genome Analysis Toolkit: a MapReduce framework for analyzing next-generation DNA sequencing data. *Genome Research*, **20**(9): 1297–1303.

Ministry of Agriculture and Rural Affairs of the People's Republic of China. 2010. NY/T 1817-2009 Test method for wool density on sheep skin: wool stemple method. Beijing: China Agriculture Press.

Mirmahmoudi R, Niknafs Z, Alba M, et al. 2017. Seasonal pattern of skin follicles activity and fibre growth in grazing fat-tailed Kermani sheep in the South of Iran. *Small Ruminant Research*, **151**: 66–71.

Moore KE, Maloney SK, Blache D. 2015. High follicle density does not decrease sweat gland density in Huacaya alpacas. *Journal of Thermal Biology*, **47**: 1–6.

Muriuki C, Bush SJ, Salavati M, et al. 2019. A mini-atlas of gene expression for the domestic goat (*Capra hircus*). *Frontiers in Genetics*, **10**: 1080.

Nixon AJ. 1993. A method for determining the activity state of hair follicles.

Biotechnic & Histochemistry, **68**(6): 316–325.
Ofori SA, Hagan JK, Kyei F. 2021. Morphometric characterization and differentiation of West African Dwarf goat populations in Ghana. *Tropical Animal Health and Production*, **53**(1): 69.
Paus R, Cotsarelis G. 1999. The biology of hair follicles. *New England Journal of Medicine*, **341**(7): 491–497.
Pertea M, Kim D, Pertea GM, et al. 2016. Transcript-level expression analysis of RNA-seq experiments with HISAT, StringTie and Ballgown. *Nature Protocols*, **11**(9): 1650–1667.
Rong YJ, Ao XF, Guo FR, et al. 2025. Genome-wide association analysis revealed candidate genes related to early growth traits in Inner Mongolia cashmere goats. *Veterinary Sciences*, **12**(3): 192.
Rong YJ, Wang XL, Na Q, et al. 2024. Genome-wide association study for cashmere traits in Inner Mongolia cashmere goat population reveals new candidate genes and haplotypes. *BMC Genomics*, **25**(1): 658.
Schneider MR, Schmidt-Ullrich R, Paus R. 2009. The hair follicle as a dynamic miniorgan. *Current Biology*, **19**(3): R132–R142.
Scobie DR, Young SR. 2000. The relationship between wool follicle density and fibre diameter is curvilinear. *Proceedings of the New Zealand Society of Animal Production*, **60**: 162–165.
Shen WT, Song ZG, Zhong X, et al. 2022. Sangerbox: a comprehensive, interaction-friendly clinical bioinformatics analysis platform. *iMeta*, **1**(3): e36.
Smedley D, Haider S, Durinck S, et al. 2015. The BioMart community portal: an innovative alternative to large, centralized data repositories. *Nucleic Acids Research*, **43**(W1): W589–W598.
Song YL, Boncompagni AC, Kim SS, et al. 2018. Regional control of hairless versus hair-bearing skin by *Dkk2*. *Cell Reports*, **25**(11): 2981–2991. e3.
Tang QZ, Gu YR, Zhou XM, et al. 2017. Comparative transcriptomics of 5 high-altitude vertebrates and their low-altitude relatives. *Gigascience*, **6**(12): gix105.
Turner SD. 2018. qqman: an R package for visualizing GWAS results using Q-Q and manhattan plots. *The Journal of Open Source Software*, **3**(25): 731.
Urban G, Feil N, Csuka E, et al. 2021. Combining deep learning with optical coherence tomography imaging to determine scalp hair and follicle counts. *Lasers in Surgery and Medicine*, **53**(1): 171–178.
Wang HJ, Cao X, Lin ZM, et al. 2015. Exome sequencing reveals mutation in *GJA1* as a cause of keratoderma-hypotrichosis-leukonychia totalis syndrome. *Human Molecular Genetics*, **24**(1): 243–250.
Wang W, Li ZH, Xie GX, et al. 2023. Convergent genomic signatures of cashmere traits: evidence for natural and artificial selection. *International Journal of Molecular Sciences*, **24**(2): 1165.
Wang ZY, Wang YR, Hui TY, et al. 2021. Single-cell sequencing reveals differential cell types in skin tissues of liaoning cashmere goats and key genes related potentially to the fineness of cashmere fiber. *Frontiers in Genetics*, **12**: 726670.
Wu CL, Yuan L, Cao WZ, et al. 2023. Regulation of secondary hair follicle cycle in cashmere goats by miR-877-3p targeting *IGFBP5* gene. *Journal of Animal Science*, **101**: skad314.
Wu P, Zhang YM, Xing YZ, et al. 2019. The balance of Bmp6 and Wnt10b regulates the telogen-anagen transition of hair follicles. *Cell Communication and Signaling*, **17**(1): 16.
Wu YT, Ru ZQ, Peng Y, et al. 2024. Peptide CyRL-QN15 accelerates hair regeneration in diabetic mice by binding to the Frizzled-7 receptor. *Zoological Research*, **45**(6): 1287–1299.
Xing WY, Deng N, Xin BJ, et al. 2019. An image-based method for the automatic recognition of cashmere and wool fibers. *Measurement*, **141**: 102–112.
Yang CH, Xu JH, Ren QC, et al. 2019. Melatonin promotes secondary hair follicle development of early postnatal cashmere goat and improves cashmere quantity and quality by enhancing antioxidant capacity and suppressing apoptosis. *Journal of Pineal Research*, **67**(1): e12569.
Yang F, Liu ZH, Zhao M, et al. 2020. Skin transcriptome reveals the periodic changes in genes underlying cashmere (ground hair) follicle transition in cashmere goats. *BMC Genomics*, **21**(1): 392.
Yang F, Ruixin Y, Xiaochun M, et al. 2023. Extremely hair follicle density is associated with a significantly different cecal microbiota in rex rabbits. *Experimental Dermatology*, **32**(9): 1361–1370.
Yang M, Song S, Dong KZ, et al. 2017. Skin transcriptome reveals the intrinsic molecular mechanisms underlying hair follicle cycling in Cashmere goats under natural and shortened photoperiod conditions. *Scientific Reports*, **7**(1): 13502.
Yang R, Zhou D, Tan XS, et al. 2024. Genome-wide association study of body conformation traits in tashi goats (*Capra hircus*). *Animals*, **14**(8): 1145.
Ye J, Coulouris G, Zaretskaya I, et al. 2012. Primer-BLAST: a tool to design target-specific primers for polymerase chain reaction. *BMC Bioinformatics*, **13**(1): 134.
Yin LL, Zhang HH, Tang ZS, et al. 2021. rMVP: a memory-efficient, visualization-enhanced, and parallel-accelerated tool for genome-wide association study. *Genomics Proteomics & Bioinformatics*, **19**(4): 619–628.
Zang LR, Xin BJ, Deng N. 2022. Identification of wool and cashmere fibers based on multiscale geometric analysis. *The Journal of the Textile Institute*, **113**(6): 1001–1008.
Zhang CZ, Sun HZ, Li SL, et al. 2018. Effects of photoperiod on nutrient digestibility, hair follicle activity and cashmere quality in Inner Mongolia white cashmere goats. *Asian-Australasian Journal of Animal Sciences*, **32**(4): 541–547.
Zhang JP, Chen ZY, Zhang SY, et al. 2025a. Spatial variation and associated genes of total hair follicle density in goats. *Animal Bioscience*, doi: https://doi.org/10.5713/ab.25.0026.
Zhang JP, Deng CC, Chen SR, et al. 2020a. Effect of body site on hair follicle density in Inner Mongolia cashmere goat (*Capra hircus*). *Small Ruminant Research*, **191**: 106164.
Zhang JP, Deng CC, Li JL, et al. 2020b. Transcriptome-based selection and validation of optimal house-keeping genes for skin research in goats (*Capra hircus*). *BMC Genomics*, **21**(1): 493.
Zhang JP, Deng CC, Zhao YJ. 2022a. Effect of number and area of view-fields on the measurement accuracy of hair follicle density in goats (*Capra hircus*). *Small Ruminant Research*, **210**: 106674.
Zhang JP, Fang JB, Zhang SY, et al. 2025b. Several variants on chromosome 10 are associated with coarse hair diameter in Dazu black goats (*Capra hircus*). *Animal Genetics*, **56**(1): e13509.
Zhang JP, Fang XQ, Zhao YJ. 2022b. The occupied proportion of hair follicle group in Inner Mongolia cashmere goat (*Capra hircus*). *Small Ruminant Research*, **210**: 106667.
Zhang YJ, Wu KJ, Wang LL, et al. 2019. Comparative study on seasonal hair follicle cycling by analysis of the transcriptomes from cashmere and milk goats. *Genomics*, **112**(1): 332–345.
Zhao B, Chen Y, Hao Y, et al. 2018. Transcriptomic analysis reveals differentially expressed genes associated with wool length in rabbit. *Animal Genetics*, **49**(5): 428–437.
Zhao YHT, Pu YB, Liang BM, et al. 2022. A study using single-locus and multi-locus genome-wide association study to identify genes associated with teat number in Hu sheep. *Animal Genetics*, **53**(2): 203–211.
Zhong YQ, Lu K, Tian J, et al. 2017. Wool/cashmere identification based on projection curves. *Textile Research Journal*, **87**(14): 1730–1741.
Zhou X, Stephens M. 2012. Genome-wide efficient mixed-model analysis for association studies. *Nature Genetics*, **44**(7): 821–824.